International Journal of Heat and Technology
Vol. 44, No. 1, February, 2026, pp. 235-243
Journal homepage: http://iieta.org/journals/ijht

Performance Analysis of a Natural Convection Solar Air Heater Operating in Ho Chi Minh City

Doan Thi Hong Hai[1], Nguyen Van Hap[2,3], Nguyen Thi Tam Thanh[1], Nguyen Minh Phu[1*]

[1] Faculty of Heat and Refrigeration Engineering, Industrial University of Ho Chi Minh City (IUH), Ho Chi Minh City 700000, Vietnam
[2] Faculty of Mechanical Engineering, Ho Chi Minh City University of Technology (HCMUT), Ho Chi Minh City 700000, Vietnam
[3] Vietnam National University Ho Chi Minh City (VNU-HCM), Ho Chi Minh City 700000, Vietnam

Corresponding Author Email: nguyenminhphu@iuh.edu.vn

https://doi.org/10.18280/ijht.440120

Received: 13 August 2025
Revised: 14 January 2026
Accepted: 30 January 2026
Available online: 28 February 2026

Keywords:
solar air collector, free convection, thermal efficiency, optimal inclination angle, experimental validation

ABSTRACT

This paper analyzes the performance of a natural convection solar air heater operating in the tropical climate of Ho Chi Minh City. We developed a mathematical model and validated it against experimental data. The model proved reliable, showing minimal discrepancies between simulated and measured temperatures. Using this validated model, a parametric study revealed that thermal efficiency increases with a larger air gap height and a shorter collector length. A critical finding for practical optimization is the determination of the optimal collector inclination angle, which varies seasonally to maximize thermal efficiency. Specifically, the optimal angle is identified as 50° to 60° for February and March, and 40° to 50° for October and December. The study concludes that this mathematical model acts as a robust tool for the design and optimization of solar air heaters in similar environments.

1. INTRODUCTION

Ho Chi Minh City has great potential for solar energy due to its location near the equator, with abundant sunshine throughout the year. The city receives an average solar radiation of about 1,581 kWh/m² per year, with the highest radiation occurring in February at 6.3 kWh/m² per day. This makes the city an ideal location for the development of solar power systems, particularly rooftop solar panels [1-4]. Ho Chi Minh City's climate is characterized as tropical monsoon, with a distinct dry season and a rainy season. This meteorological profile is shared by several cities around the world that are also located in tropical latitudes and are influenced by monsoon winds. A natural convection (or thermosiphon) solar air heater is a simple, effective device. It uses solar energy to heat air without mechanical parts like fans or pumps [5]. This system relies on a basic scientific principle: hot air is less dense than cold air, causing it to rise. The heater typically consists of a glazed collector box with a dark absorber plate inside. When sunlight hits the collector, the absorber plate heats up and transfers its heat to the air inside. As the air warms, it naturally rises and flows out of a vent at the top of the collector, while cooler, denser air from the bottom of the room is drawn in to take its place. This continuous cycle creates a natural airflow, providing either a source of warm air for heating a space or a steady supply of fresh, ventilated air [6-8]. Because it operates passively, this type of solar heater is highly reliable, silent, and has no operating costs.

A foundational study by Ong and Than [9] proposed a comprehensive theoretical model for a flat-plate solar air heater. This model, which was validated experimentally, considered heat transfer processes, including radiation and convection, and the buoyancy-driven airflow. It established the relationship between factors like tilt angle, solar radiation, and the resulting air velocity and temperature increase. This work highlights the importance of a validated mathematical framework for predicting system performance. Brinkworth [10] also provides a detailed procedure for determining flow and heat transfer in inclined cooling ducts, which can be applied to solar air heaters. The paper emphasizes the need to account for both free convection (buoyancy) and mixed-flow conditions induced by wind, and it presents a dimensionless solution for a parallel-plate duct. Several papers explore modifications to the absorber plate to enhance heat transfer and thermal efficiency. Hosseini et al. [11] investigate the use of longitudinal fins, showing a substantial improvement in thermal efficiency by increasing the heat exchange area. Expanding on this, the authors [12] compare the performance of rectangular, triangular, and elliptical fins. This research found that rectangular fins yielded the best thermal performance, despite a lower mass flow rate, and identified the optimal inclination angles for each fin shape. The use of turbulators, such as V-shaped ribs and perforated baffles, is also mentioned in other papers as an effective method to enhance the Nusselt number and thermal efficiency by increasing turbulence. The principle of natural convection is also a key mechanism in solar chimneys for passive ventilation. Mathur and Anupma [13] investigated the effect of the

absorber inclination on airflow. It concludes that the optimum inclination angle, which varies with latitude, can significantly enhance the rate of ventilation, providing a sustainable solution for cooling buildings during summer. Oria and Palconit [14] conducted a study in the tropical climate of Sultan Kudarat, Philippines. This study evaluates an inflatable solar dryer integrated with a low-cost solar air heater constructed from recycled steel cans to boost inlet temperatures. The findings confirm that this simple heater design significantly accelerates drying rates, achieving the target moisture content for coffee and corn in 27 and 8 hours, respectively, compared to 47 and 14 hours for open sun drying. Safitra et al. [15] demonstrated that integrating rectangular fins into a solar air heater located in Surabaya (Indonesia) with a ventilator turbine significantly improves thermal performance, achieving up to 29.67% higher efficiency than a finless design. The research highlights that a 30° inclination angle optimizes solar radiation absorption for this tropical latitude, effectively enhancing the system's useful heat gain under low air velocity conditions. Prasopsuk et al. [16] tested the novel design of a solar air heater in Lopburi, Thailand. This research reveals that equipping a solar air heater with tree-like fractal cylindrical pins increases thermal efficiency by 44% to 85% compared to conventional flat-plate systems. The study confirms that these fractal turbulators significantly enhance convective heat transfer and drying efficiency for agricultural products under real tropical climatic conditions.

Although previous studies established the fundamental principles of natural convection solar air heaters, they have not thoroughly analyzed their performance in specific tropical climates like Ho Chi Minh City. This research bridges that gap by developing and validating a mathematical model tailored to this environment, specifically addressing the critical need for accurately predicting induced airflow rates - a vital factor for determining thermal efficiency. Unlike existing literature, which often lacks comprehensive integration of regional meteorological data, this study incorporates a validated solar radiation model to capture specific local conditions. By shifting from theoretical generalization to localized, actionable optimization, this work provides a robust analytical tool for designing efficient systems in similar tropical settings.

2. MATHEMATICAL MODELING

Figure 1 shows a schematic diagram of a natural convection solar air heater used in this analytical study. The diagram illustrates how air flows through the collector, which consists of a glass cover, an absorber plate, and insulation. The device is tilted at an angle θ relative to the ground. Solar radiation, represented by the vector I, strikes the tilted glass surface. The diagram also indicates the inlet and outlet air positions with elevations z_1 and z_2, respectively. Air enters the channel at the lower end and exits at the higher end, driven by natural convection [17, 18].

2.1 Energy balance equations

- Energy balance equation for glass cover:

$$\alpha_g I_t = h_w\left(T_g - T_a\right) + h_{r,g,s}\left(T_g - T_s\right) + h_{c,g,f}\left(T_g - T_f\right) + h_{r,g,p}\left(T_g - T_p\right) \quad (1)$$

where, I_t is the average radiation on tilted surface, α_g is absorptivity of glass cover, h_w is convection heat transfer coefficient due to wind, T_g is mean temperature of glass, T_a is ambient temperature (inlet temperature), $h_{r,g,s}$ is radiation heat transfer coefficient between glass and sky, $h_{r,g,p}$ is radiation heat transfer coefficient between glass and absorber plate, $h_{c,g,f}$ is convection heat transfer coefficient between glass and airflow, T_f is mean temperature of air, T_p is mean temperature of absorber plate, T_s is sky temperature.

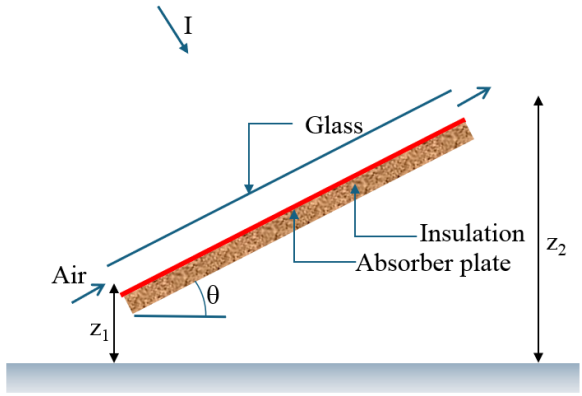

Figure 1. The natural convection solar air heater studied analytically and experimentally in the current work

- Energy balance equation for the airflow:

$$Q = Lbh_{c,g,f}\left(T_g - T_f\right) + Lbh_{c,p,f}\left(T_p - T_f\right) \quad (2)$$

$$Q = \dot{m}c_p(T_o - T_a) \quad (3)$$

where, Q is useful heat gain, L is collector length, b is collector width, $\dot{m}$ is air mass flow rate, c_p is specific heat of air, T_o is outlet air temperature, $h_{c,p,f}$ is convection heat transfer coefficient between the plate and airflow.

- Energy balance equation for absorber plate:

$$\alpha_p \tau_g I_t = h_{c,p,f}\left(T_p - T_f\right) + h_{r,g,p}\left(T_p - T_g\right) + h_b\left(T_p - T_a\right) \quad (4)$$

where, α_p is the absorptivity of the plate, τ_g is the transmissivity of the glass cover, and h_b is the convection heat transfer coefficient between the plate and the environment (heat loss through the insulation).

2.2 Induced air flow rate

Applying Bernoulli's equation to the airflow channel from the inlet (location 1) to the outlet (location 2), as shown in Figure 1 [19]:

$$z_1\rho_1 g + p_1 + \frac{\rho_1 v_1^2}{2} = z_2\rho_2 g + p_2 + \frac{\rho_2 v_2^2}{2} + f\frac{L}{D_h}\frac{\rho v^2}{2} + K_1\frac{\rho_1 v_1^2}{2} + K_2\frac{\rho_2 v_2^2}{2} + K_3\frac{\rho v^2}{2} \quad (5)$$

Since both the inlet and outlet vents are open to the atmosphere, the pressure at these points is equal to atmospheric pressure ($p_1 = p_2$). The air enters the inlet from the

atmosphere, which is considered an infinite reservoir with a negligible initial velocity ($v_1 = 0$). Hence, Eq. (5) is reduced to:

$$z_1\rho_1 g - z_2\rho_2 g = \frac{\rho_2 v_2^2}{2} + f\frac{L}{D_h}\frac{\rho v^2}{2} + K_2\frac{\rho_2 v_2^2}{2} + K_3\frac{\rho v^2}{2} \quad (6)$$

where, z is elevation, ρ is air density, g is gravitational acceleration, f is friction factor, D_h is hydraulic diameter, K_2 and K_3 are the loss coefficients at the outlet and other losses of the channel, respectively. $K_2 = 1$ and $K_3 = 1.1$ [20].

$$z_1\rho_1 g - z_2\rho_2 g = 2\frac{\rho_2 v_2^2}{2} + f\frac{L}{D_h}\frac{\rho v^2}{2} + 1.1\frac{\rho v^2}{2} \quad (7)$$

Using Boussinesq approximation: $\rho_1 = \rho\beta T_a$ and $\rho_2 = \rho\beta T_o$. And assume $v_2 = v$:

$$gL\sin(\theta)\beta(T_o - T_a)\rho = \frac{1}{2}\left(2\rho\beta T_o v^2 + f\frac{L}{D_h}\rho v^2 + 1.1\rho v^2\right) \quad (8)$$

where, β is the thermal expansivity of air, $\beta = 1/T_f$ in which $T_f = 0.25T_a + 0.75T_o$ [20], θ is the inclination angle of the collector. Therefore, air velocity inside the channel can be estimated as:

$$v^2 = 2g\beta L sin(\theta)(T_o - T_a)(1.1 + fL/D_h + 2\beta T_o)^{-1} \quad (9)$$

Hydraulic diameter:

$$D_h = \frac{4Hb}{2(H+b)} \quad (10)$$

The friction factor (f) for laminar and turbulent flows is calculated by the following correlations, respectively:

$$f = 1.906(Gr/Pr)^{1/12} \quad (11)$$

$$f = 1.368(Gr/Pr)^{1/11.9} \quad (12)$$

where, Pr is the Prandtl number of air.

Grashof number:

$$Gr = g\beta(T_p - T_g)L^3\frac{\rho^2}{\mu^2} \quad (13)$$

2.3 Solar radiation on the inclined collector

The Liu and Jordan model is an isotropic model that simplifies solar radiation by assuming diffuse radiation is uniformly distributed across the sky. It is a foundational method for estimating the solar radiation incident on a tilted surface by using global horizontal radiation data. This model is particularly useful for predicting solar energy in cloudy weather conditions and has been applied in various studies to determine the optimal tilt angle for solar collectors. Average radiation on a sloped surface is evaluated by the method of Liu and Jordan as [21, 22]:

$$I_t = I(1 - I_d/I)R_b + I(I_d/I)\frac{1+\cos(\theta)}{2} + I\rho_g\frac{1-\cos(\theta)}{2} \quad (14)$$

where, R_b is the ratio of the average beam radiation on the tilted surface to that on a horizontal surface, I_d is diffuse radiation, ρ_g is ground reflectance.

$$R_b = \frac{\cos(\phi-\theta)\cos(\delta)sin(\omega_s') + (\pi\omega_s'/180)sin(\phi-\theta)sin(\delta)}{\cos(\phi)\cos(\delta)sin(\omega_s) + (\pi\omega_s/180)sin(\phi)sin(\delta)} \quad (15)$$

where, ϕ is latitude, ω_s is the sunset hour angle, ω_s' is the sunset hour angle for the tilted surface, δ is solar declination.

$$\delta = 23.45sin\left(360\frac{284+n}{365}\right) \quad (16)$$

where, n is the day number of the year.

$$\omega_s = arccos\left(-sin(\phi)\frac{sin(\delta)}{cos(\phi)cos(\delta)}\right) \quad (17)$$

$$\omega_s' = min\begin{bmatrix} arccos(-tan(\phi)tan(\delta)) \\ arccos(-tan(\phi-\theta)tan(\delta)) \end{bmatrix} \quad (18)$$

I_d/I in Eq. (14) is a function of the clearness index $\bar{K}_T$ as:

$$I_d/I = 1.391 - 3.56\bar{K}_T + 4.189\bar{K}_T^2 - 2.137\bar{K}_T^3 \quad (19)$$

for $\omega_s < 81.4°$:

$$I_d/I = 1.311 - 3.022\bar{K}_T + 3.427\bar{K}_T^2 - 1.821\bar{K}_T^3 \quad (20)$$

for $\omega_s > 81.4°$:

$$\bar{K}_T = I/I_o \quad (21)$$

where, I_o is the extraterrestrial radiation on a horizontal surface.

$$I_o = \frac{G_{SC}}{\pi}\left(1 + 0.033\cos\frac{360n}{365}\right)\times \left(\cos(\delta)\cos(\phi)sin(\omega_s) + \frac{\pi\omega_s}{180}sin(\delta)sin(\phi)\right) \quad (22)$$

where, G_{SC} is the solar constant, $G_{SC} = 1367$ W/m^2.

2.4 Other equations

Heat transfer coefficient due to wind is estimated by the McAdam equation [23]:

$$h_w = 5.7 + 3.8V_w \quad (23)$$

where, V_w is wind velocity.

Sky temperature [24]:

$$T_s = 0.0552T_a^{1.5} \quad (24)$$

where, T_a is the ambient temperature.

The heat transfer coefficient between the air flow in the channel and the glass ($h_{c,g,f}$), and the heat transfer coefficient between the air flow in the channel and the absorber plate ($h_{c,p,f}$), are supposed equal and are given by [20]:

$$h_{c,g,f} = \left(0.68 + 0.67 \frac{Ra^{0.25}}{\left(1 + \left(0.492 / Pr\right)^{9/16}\right)^{4/9}} \right) k / L \quad (25)$$

for laminar flow ($Ra < 10^9$):

$$h_{c,g,f} = \left(0.825 + 0.39 \frac{Ra^{1/6}}{\left(1 + \left(0.492 / Pr\right)^{9/16}\right)^{8/27}} \right)^2 k / L \quad (26)$$

for turbulent flow ($Ra > 10^9$).

where, Ra is the Rayleigh number (Ra = GrPr), k is the thermal conductivity of air.

The radiation heat transfer coefficient between the glass and the sky:

$$h_{r,g,s} = \sigma \varepsilon_g \left(T_g^{\,2} + T_s^{\,2}\right)\left(T_g + T_s\right) \quad (27)$$

where, ε_g is the emissivity of glass, σ is Stefan's constant.

The radiation heat transfer coefficient between the glass and the absorber plate:

$$h_{r,g,p} = \sigma\left(T_g^{\,2} + T_p^{\,2}\right)\frac{T_g + T_p}{1/\varepsilon_g + 1/\varepsilon_p - 1} \quad (28)$$

where, ε_p is the emissivity of the absorber plate.

Convection heat transfer coefficient between the plate and the environment:

$$h_b = k_i / t_i \quad (29)$$

where, t_i is the insulation thickness, and k_i is the thermal conductivity of insulation.

Induced air mass flow rate:

$$\dot{m} = \rho v b H \quad (30)$$

where, H is the air channel height.

Thermal efficiency of the natural solar air heater:

$$\eta = \frac{Q}{LbI_t} \quad (31)$$

Temperature effectiveness [25]:

$$\varepsilon = \frac{T_o - T_a}{T_p - T_a} \quad (32)$$

Table 1 shows the parameters entered into the simulation program. The radiation to the inclined collector is calculated from the monthly average horizontal radiation at Ho Chi Minh City, given in Table 2. This data is averaged from the weather data distributed with TRNSYS simulation software. The mathematical model above is written in EES (F-chart software), which is good at dealing with nonlinear algebraic equations.

Table 1. Input parameters

Parameter	Value
Latitude (Ho Chi Minh City)	ϕ = 10°
Ground reflectance	ρ_g = 0.2
Absorptivity of glass cover	α_g = 0.06
Transmissivity of glass cover	τ_g = 0.84
Emissivity of absorber plate	ε_g = 0.95
Emissivity of glass	ε_g = 0.86
Insulation thickness	m t_i = 0.05 m
Thermal conductivity of insulation	k_i = 0.025 W/m K
Wind velocity	V_w = 1 m/s
Ambient temperature	T_a = 300 K

Table 2. Average total radiation on a horizontal surface (I) in Ho Chi Minh City

Month	I (W/m^2)
January	560.46
February	522.63
March	553.59
April	468.27
May	542.53
June	511.48
July	518.53
August	523.36
September	358.00
October	425.19
November	425.46
December	494.27

3. EXPERIMENTAL VALIDATION

This section details the physical setup and measurements taken for the solar air heater as shown in Figure 2. The collector is tilted at an angle of θ = 20° and located in Ho Chi Minh City. The image on the right provides a cross-sectional view of the collector, highlighting its internal components. It shows the glass cover, the air channel with a height of H = 30 mm, the absorber plate, and the insulation beneath it. An experiment was conducted for one hour, from 10 AM to 11 AM, on July 25, 2025. The solar radiation was measured using a solar power meter TES 132 and was relatively constant at I = 450 W/m^2 during the test period. This specific time window was selected because solar radiation was relatively constant and ambient conditions were stable. This stability ensured quasi-steady-state conditions. These conditions are essential for validating heat transfer correlations and friction factors without interference from transient thermal inertia. The glass temperature was measured with a thermal imaging camera Hti HT-18+, while the absorber plate temperature was measured with a 4-channel temperature meter Extech SDL200. The experimental results showed that the glass temperature fluctuated around 40 °C as shown in Figure 3, and the average absorber plate temperature was 73.7 °C. These experimental values were then compared to the simulation results from the above mathematical modeling, which predicted a glass temperature of 315.1 K (or 41.95 °C) and an absorber plate temperature of 348.4 K (or 75.25 °C). The discrepancies between the mathematical model and the experimental results are minimal, indicating that the model is reliable for

conducting parametric studies. The close agreement between the simulated and measured temperatures validates the model's accuracy, making it a trustworthy tool for further analysis.

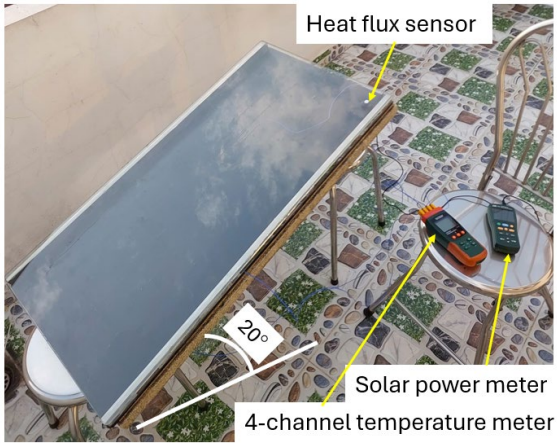

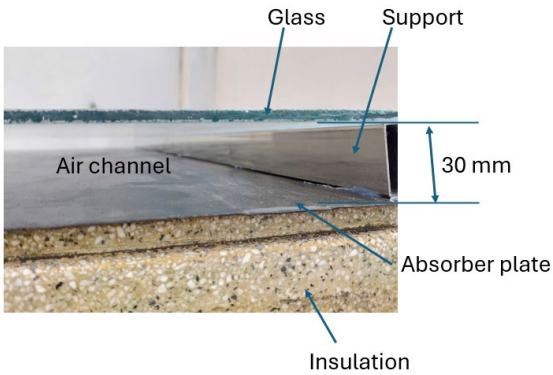

Figure 2. Experimental setup

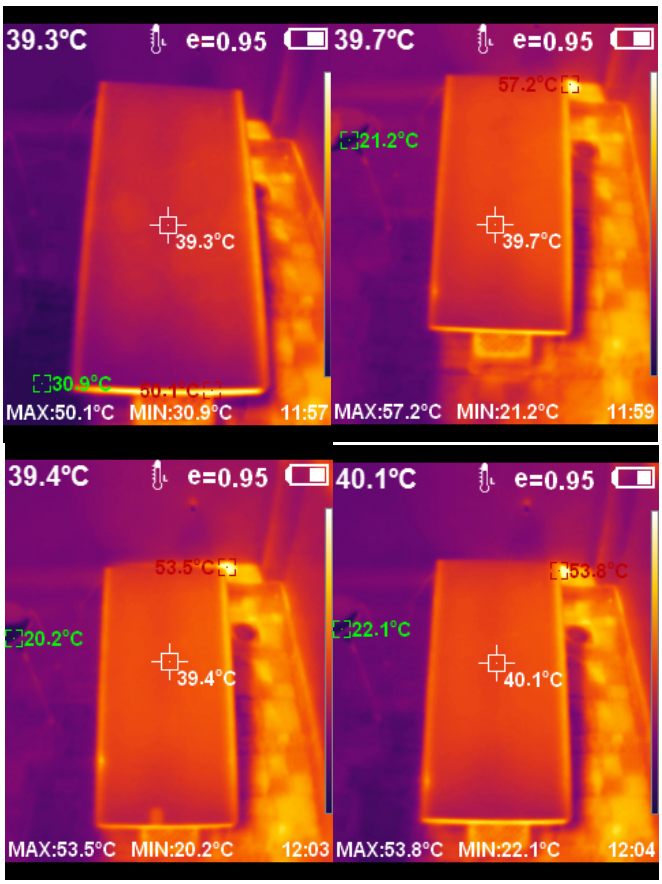

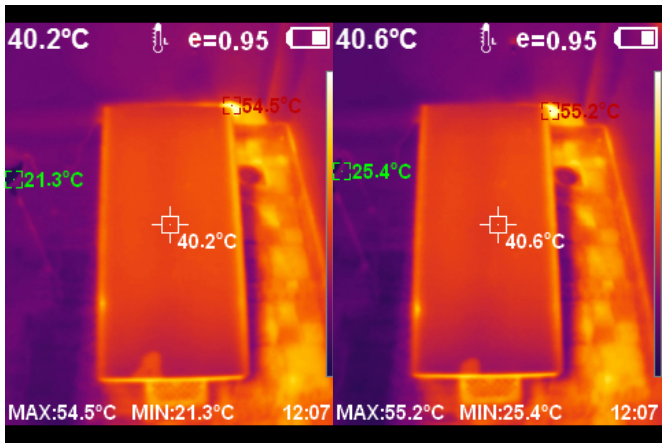

Figure 3. Glass temperature taken by thermal imaging camera

4. RESULTS AND DISCUSSION

Figure 4 illustrates the average solar radiation on the inclined collector (I_t) as a function of the inclination angle (θ) for four typical months: January, March, September, and November. The tilted surface radiation is calculated using the Liu and Jordan model, which is described in Section 2.3. The input for the model is the monthly average total radiation on a horizontal surface (I), which is provided in Table 2. The graph shows that for each month, there is an optimal inclination angle that maximizes the solar radiation received. For January, the maximum radiation is around a 35° inclination angle, while for March and November, the peak is at a slightly lower angle. For September, the radiation is generally lower, and the optimal angle is less pronounced. These results demonstrate how the optimal tilt angle for the collector changes depending on the month due to the sun's position.

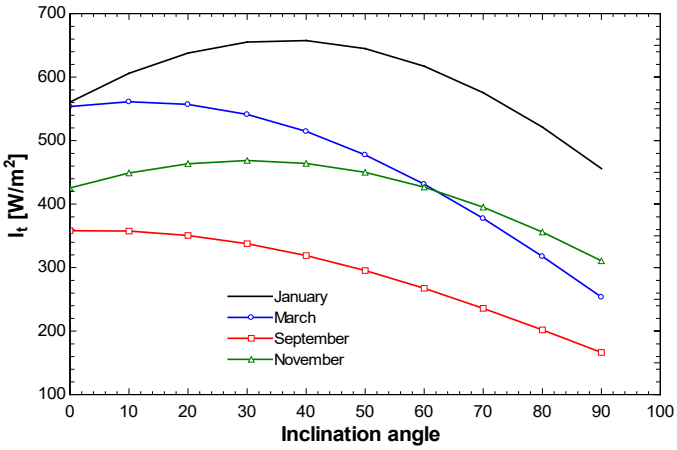

Figure 4. Solar radiation on the inclined collector for typical months

Figure 5 qualitatively shows that the induced air mass flow rate is influenced by both the air gap height (H) and the collector inclination angle (θ) in February with L = 1 m. Quantitatively, the results indicate that a larger air gap height leads to a higher mass flow rate. At a 65° inclination, the mass flow rate peaked at roughly 0.0043 kg/s for H = 100 mm. This exceeded rates for H = 65 mm (0.0042 kg/s) and H = 30 mm (0.0040 kg/s). A larger air channel provides less resistance to the airflow, allowing a greater volume of air to circulate for

the same driving force of natural convection. The graph also shows that for each air gap height, there is an optimal inclination angle that maximizes the flow rate, which for all three cases appears to be between 60° and 70°. This is because the natural convection driving force, which is a function of the temperature difference and the vertical height difference (z_2-z_1), is maximized at this angle, while frictional losses also play a role.

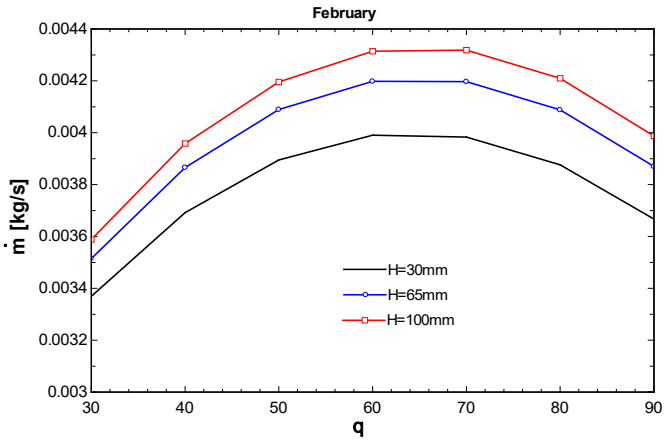

Figure 5. Effect of air gap height and collector inclination on induced air flow rate

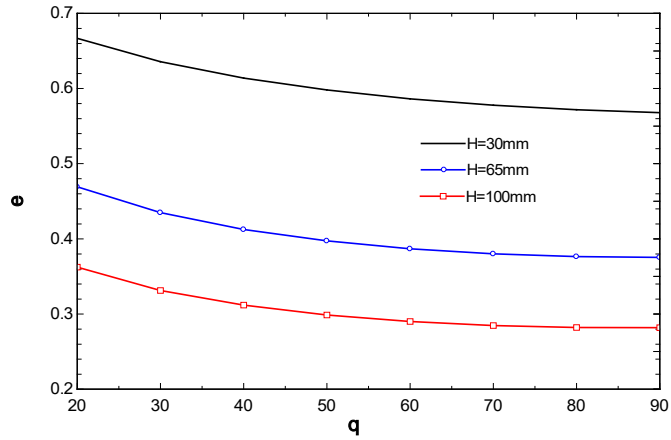

Figure 6. Effect of air gap height and collector inclination on temperature effectiveness

Figure 6 demonstrates the relationship between temperature effectiveness (ε), air gap height (H), and collector inclination angle (θ). The graph shows that a smaller air gap height results in a higher temperature effectiveness. The curve for H = 30 mm is consistently above the curves for H = 65 mm and H = 100 mm, indicating a greater temperature effectiveness. For a given amount of heat transferred to the air, a smaller air channel forces the air to absorb the heat more intensely, leading to a larger temperature increase. As a result, the outlet air temperature (T_o) becomes significantly higher relative to the ambient temperature (T_a) and the absorber plate temperature (T_p), as defined by the temperature effectiveness formula (32). Temperature effectiveness drops as the inclination angle increases. This occurs primarily because the natural convection airflow rate decreases. As the angle of inclination increases, the component of gravity that drives the buoyant air upward along the channel decreases, reducing the air velocity. A lower air velocity results in a lower mass flow rate, which in turn reduces the amount of useful heat gained by the air for a given solar radiation input. Additionally, as the inclination angle increases, the solar radiation absorbed by the collector may also decrease after a certain optimal angle is reached, further lowering the overall heat transfer to the air.

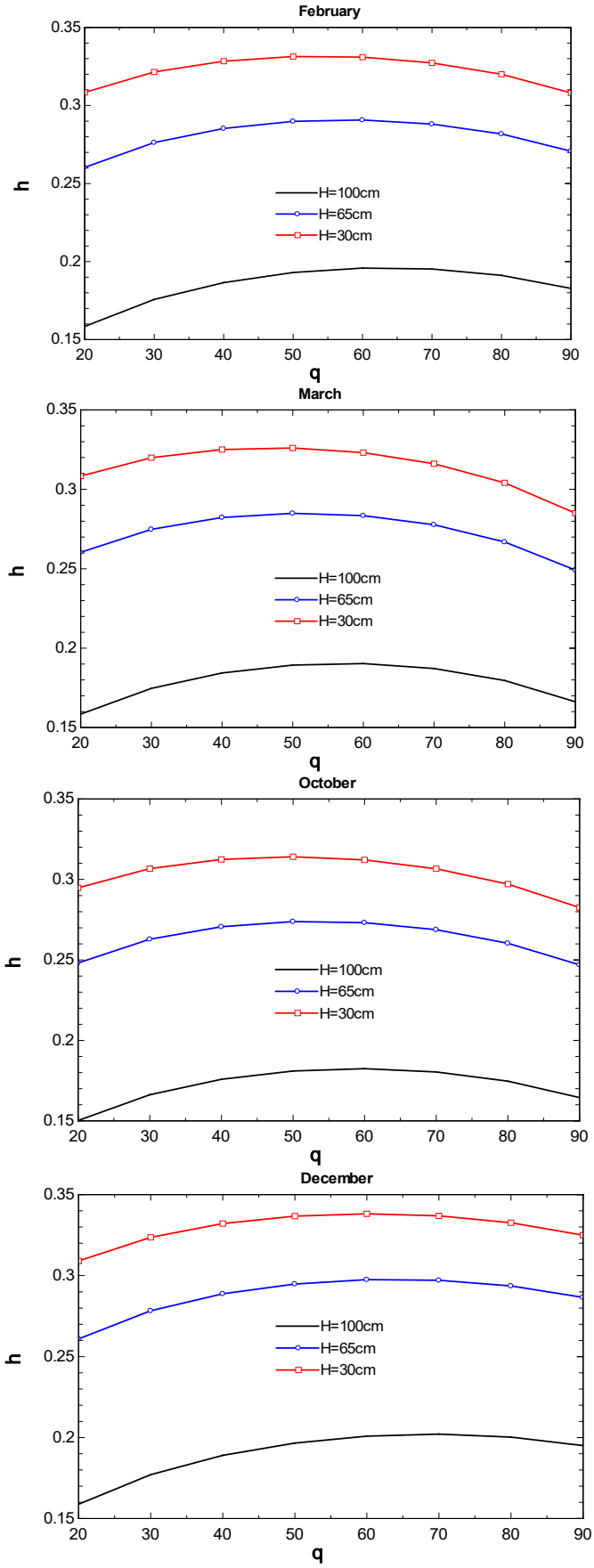

Figure 7. Effect of air gap height, month and collector inclination on thermal efficiency

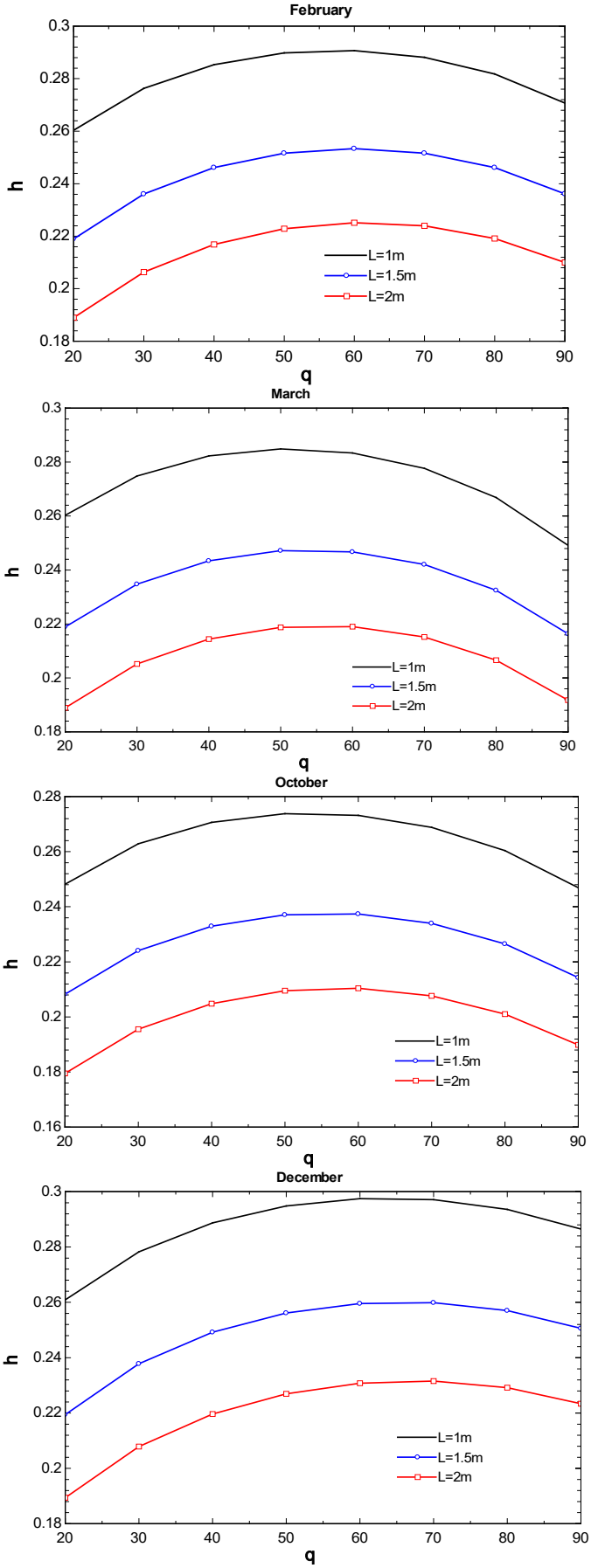

Figure 8. Effect of collector length (L) when fixing H = 65 cm

Figure 7 demonstrates the effect of air gap height (H), month, and collector inclination (θ) on thermal efficiency (η). The graphs for February, March, October, and December all show a consistent trend: for a given month and inclination angle, a larger air gap height (H) leads to a higher thermal efficiency. In the February graph, the thermal efficiency for H = 100 cm is significantly higher than for H = 30 cm. As seen in Figure 5, a larger air gap height leads to a higher air mass flow rate, which in turn increases the useful heat gain. While a larger H results in a lower temperature effectiveness (as per Figure 6), the increased mass flow rate from the larger channel size outweighs this effect, leading to a higher overall thermal efficiency. The graphs also show that for each case, there is an optimal inclination angle that maximizes the thermal efficiency, which varies with the month due to changes in solar radiation. Figure 7 shows that the optimal inclination angle for thermal efficiency varies significantly by month. For February and March, the thermal efficiency peaks at an inclination angle between 50° and 60° degrees for all air gap heights (H = 30 cm, H = 65 cm, and H = 100 cm). This suggests that for months with a higher sun angle, a steeper collector tilt is required to achieve the best performance. In contrast, for October and December, the optimal inclination angle is lower, typically between 40° and 50°. This is consistent with the sun's lower position in the sky during these months, where a shallower angle is needed to capture a greater amount of solar radiation. The graphs clearly show that to maximize the thermal efficiency of the solar air heater, the inclination angle should be adjusted seasonally to align with the sun's position.

Figure 8 examines the impact of collector length (L) on thermal efficiency (η) for a fixed air gap height of H = 65 cm across several months (February, March, October, and December). It shows that a shorter collector length leads to a higher thermal efficiency. For any given month and inclination angle, the thermal efficiency for a collector length of L = 1 m is the highest, followed by L = 1.5 m, and then L = 2 m. In February, at an inclination angle of 60°, the thermal efficiency is highest for L = 1 m, and lowest for L = 2 m. This is because a longer channel increases frictional losses, which reduces the induced air mass flow rate for a given temperature difference. While a longer collector can absorb more solar energy, the reduced air flow rate due to increased channel friction means that the air heats up less effectively along its path, leading to a lower overall thermal efficiency. As with the other figures, each graph also shows an optimal inclination angle for thermal efficiency, which varies by month.

5. CONCLUSIONS

This study developed and validated a mathematical model for a natural convection solar air heater operating in Ho Chi Minh City. The model demonstrated high reliability in predicting system temperatures under steady-state conditions, serving as a robust tool for parametric optimization. The analysis highlights the practical necessity of a seasonally adjustable inclination strategy over a fixed-tilt approach to maximize annual performance. To maintain peak thermal efficiency in this tropical latitude, the collector inclination should be adjusted dynamically: higher angles (50°–60°) are required during the high-irradiance months of February and March, while lower angles (40°–50°) are optimal for October and December. Geometric optimization shows that increasing the air gap height and reducing the collector length lowers flow resistance. This enhances both induced airflow and overall thermal efficiency.

Future work will focus on long-term experimental monitoring to assess dynamic responses to fluctuating irradiance and investigate the integration of heat transfer enhancements, such as fins or turbulators, to further improve system performance.

ACKNOWLEDGMENT

The author Nguyen Van Hap acknowledges Ho Chi Minh City University of Technology (HCMUT), VNU-HCM, for supporting this study.

REFERENCES

[1] Thanh, N.V., Lan, N.T.K. (2022). Solar energy deployment for the sustainable future of Vietnam: Hybrid SWOC-FAHP-WASPAS analysis. Energies, 15(8): 2798. https://doi.org/10.3390/en15082798

[2] Minh, P.V., Le Quang, S., Pham, M.H. (2021). Technical economic analysis of photovoltaic-powered electric vehicle charging stations under different solar irradiation conditions in Vietnam. Sustainability, 13(6): 3528. https://doi.org/10.3390/su13063528

[3] Van Hap, N., Dam, M.T., Khoi, N.H., Phu, N.M. (2024). Parametric investigation and optimization of the photovoltaic-thermal air heater. Journal of Advanced Research in Fluid Mechanics and Thermal Sciences, 120(2): 67-81. https://doi.org/10.37934/arfmts.120.2.6781

[4] Rozak, O.A., Ibrahim, M.Z., Daud, M.Z., Bakhri, S., Oktavian, T.E. (2024). Case study of the effect of tilt angle on output power and efficiency of photovoltaic using two solar irradiation measurement methods. Journal of Advanced Research in Applied Sciences and Engineering Technology, 38(1): 25-36. https://doi.org/10.37934/araset.38.1.2536

[5] Fath, H.E. (1995). Transient analysis of thermosyphon solar air heater with built-in latent heat thermal energy storage system. Renewable Energy, 6(2): 119-124. https://doi.org/10.1016/0960-1481(94)00050-G

[6] Nguyen Minh, P., Nguyen Hoang, K., Nguyen Van, H. (2022). Impact of the V cap on induced turbulent air flow in a solar chimney: A computational study. Journal of Thermal Engineering, 9: 1-12.

[7] Hau, C.T., Hai, D.T.H., Hap, N.V., Phu, N.M. (2021). One-dimensional and entropy generation analyses of a solar chimney. In the AUN/SEED-Net Joint Regional Conference in Transportation, Energy, and Mechanical Manufacturing Engineering, pp. 211-219. https://doi.org/10.1007/978-981-19-1968-8_17

[8] Samsudin, S.S.A., Shaari, A.M., Abdullah, K., Batcha, M.F.M. (2020). Potential of utilizing solar chimney as an energy efficiency measure in Malaysian hospitals. CFD Letters, 12(4): 90-99. https://doi.org/10.37934/cfdl.12.4.9099

[9] Ong, K., Than C.F. (2005). A theoretical model of a natural convection solar air heater. In Solar 2005 Conference, Australian and New Zealand Solar Energy Society (ANZSES), Otago University, Dunedin, New Zealand.

[10] Brinkworth, B. (2000). Estimation of flow and heat transfer for the design of PV cooling ducts. Solar Energy, 69(5): 413-420. https://doi.org/10.1016/S0038-092X(00)00082-7

[11] Hosseini, S.S., Ramiar, A., Ranjbar, A.A. (2019). The effect of fins shadow on natural convection solar air heater. International Journal of Thermal Sciences, 142: 280-294. https://doi.org/10.1016/j.ijthermalsci.2019.04.015

[12] Hosseini, S.S., Ramiar, A., Ranjbar, A.A. (2018). Numerical investigation of natural convection solar air heater with different fins shape. Renewable Energy, 117: 488-500. https://doi.org/10.1016/j.renene.2017.10.052

[13] Mathur, J., Anupma, M.S. (2006). Summer-performance of inclined roof solar chimney for natural ventilation. Energy and Buildings, 38(10): 1156-1163. https://doi.org/10.1016/j.enbuild.2006.01.006

[14] Oria, C.L., Palconit, E.V. (2022). Performance investigation of an inflatable solar dryer with steel-can solar air heater for drying coffee and corn. Engineering, Technology & Applied Science Research, 12(3): 8707-8711. https://doi.org/10.48084/etasr.4966

[15] Safitra, A.G., Diana, L., Arini, N.R., Agil, D.M., Farezza, J.H. (2020). Thermal analysis of solar air heater with ventilator turbine and fins. EMITTER International Journal of Engineering Technology, 8(2): 510-523. https://doi.org/10.24003/emitter.v8i2.584

[16] Prasopsuk, C., Sutthivirode, K., Thongtip, T. (2025). Performance enhancement of a solar air heater equipped with a tree-like fractal cylindrical pin for drying applications: Tests under real climatic conditions. Energies, 18(9): 2230. https://doi.org/10.3390/en18092230

[17] Hai, D.T.H., Phu, N.M. (2023). A critical review of all mathematical models developed for solar air heater analysis. Journal of Advanced Research in Fluid Mechanics and Thermal Sciences, 105(1): 1-14. https://doi.org/10.37934/arfmts.105.1.114

[18] Van Hung, T., Ngo, T.T., Phu, N.M. (2025). A computational solution of melting process inside a sphere towards the latent heat storage in a solar air heater. CFD Letters, 17(7): 61-73. https://doi.org/10.37934/cfdl.17.7.6173

[19] Tonui, J., Tripanagnostopoulos, Y. (2008). Performance improvement of PV/T solar collectors with natural air flow operation. Solar Energy, 82(1): 1-12. https://doi.org/10.1016/j.solener.2007.06.004

[20] Bahrehmand, D., Ameri, M., Gholampour, M. (2015). Energy and exergy analysis of different solar air collector systems with forced convection. Renewable Energy, 83: 1119-1130. https://doi.org/10.1016/j.renene.2015.03.009

[21] Duffie, J.A., Beckman, W.A. (2013). Solar Engineering of Thermal Processes. John Wiley & Sons. https://doi.org/10.1002/9781118671603

[22] Khan, M.S., Ramli, M.A.M., Sindi, H.F., Hidayat, T., Bouchekara, H.R.E.H. (2022). Estimation of solar radiation on a PV panel surface with an optimal tilt angle using electric charged particles optimization. Electronics, 11(13): 2056. https://doi.org/10.3390/electronics11132056

[23] Shemelin, V., Matuška, T. (2023). The effect of the wind conditions on the thermal performance of an unglazed solar thermal collector. Energy Reports, 10: 2880-2888. https://doi.org/10.1016/j.egyr.2023.09.132

[24] Phu, N.M., Tu, N.T., Hap, N.V. (2021).

Thermohydraulic performance and entropy generation of a triple-pass solar air heater with three inlets. Energies, 14(19): 6399. https://doi.org/10.3390/en14196399
[25] Singh, A.P., Kumar, A., Singh, O. (2021). Natural convection solar air heater: Bell-mouth integrated converging channel for high flow applications. Building and Environment, 187: 107367. https://doi.org/10.1016/j.buildenv.2020.107367